Nuclear Instruments and Methods in Physics Research A 384 (1997) 351-359

ELSEVIER

NUCLEAR INSTRUMENTS & METHODS IN PHYSICS RESEARCH Section A

Performance of MSGC with analog pipeline readout ★

F. Gómez *, B. Adeva, G. Gracia, M.A. López, T. Núñez, A. Pazos, M. Pló, A. Rodríguez, C. Santamarina, P. Vázquez

Universidad de Santiago de Compostela, 15706 Santiago, Spain

Received 31 May 1996; revised form received 29 September 1996

Abstract

We analyse some of the performance characteristics of a chromium MSGC operated with Ar–DME 50%–50% in a test beam at CERN. Excellent signal-to-noise ratio and efficiency has been achieved with this gas mixture using cathode analog pipeline readout. We also determine optimal parameters for the sampling algorithm in order to work in a random trigger experiment (fixed target).

1. Introduction

We report here on the results obtained in a test beam at CERN PS with a Microstrip Gas Chamber (MSGC) prototype, whose parameters will be described later. The motivation of the test beam was to study the performance of a MSGC and a scintillating fiber detector for background rejection of $\pi^+\pi^-$ pairs, in the framework of the DIRAC experiment [1]. The operation of these detectors has been intensively studied and used for minimum ionizing particle (MIP) detection [2,3]. Recent developments in substrate passivation [4,5] and in strip metallization [6,7] have shown a good aging behaviour [8–10] (up to 100 mC/cm) and a strong rate capability of the order of 10^6 mm^{-2}s^{-1}.

2. Experimental setup

The detector performance was tested in the PS beam at CERN in October 1995. The setup of the combined detectors is shown in Fig. 1. The MSGC plane was built on a DESAG D263 substrate with implanted chromium strips [1] (10 μm and 100 μm width for anodes and cathodes, respectively). The detector mask was designed to perform readout of cathode strip signals. The gas mixture was set to 50%–50% Ar–DME with a gas gap of 3 mm height. The operation voltages were −2 kV for the drift electrode and +590 V for anodes, cathodes and backplane being grounded. An overall detector gain of approximately 3000 was achieved in this way.

3. Readout electronics

We implemented as front-end electronics two Analog Pipeline Chips, APC [11,12] with 64 channels each. A channel consists of a charge sensitive preamplifier followed by a 32 analog buffer pipeline which ends in a

★ Work supported by Comisión Interministerial de Ciencia y Tecnología (CICYT), projects AEN93–0602, AEN94–0573.

* Corresponding author. Tel: +34 81 521091, fax: +34 81 520676, e-mail: faustino@gaes.usc.es. Departamento de Física de Partículas, Univ. de Santiago, Campus Sur s/n, 15706 Santiago, Spain.

[1] The mask was provided by the CERN GDD group and production of the MSGC was performed by IMT Greinfensee (Switzerland).

PII S0168-9002(96)00943-6

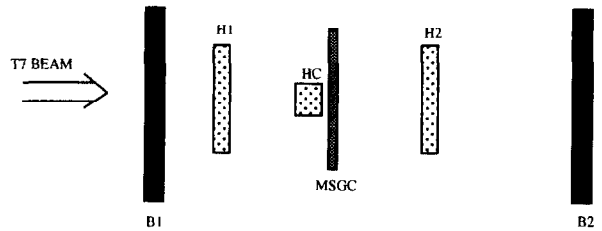

Fig. 1. Experimental setup. B1 and B2 beam counters. HC scintillating fiber hodoscope with multi-anode readout. H1 and H2 scintillating fiber hodoscopes with delay line readout. HC detector was 5 cm upstream of MSGC.

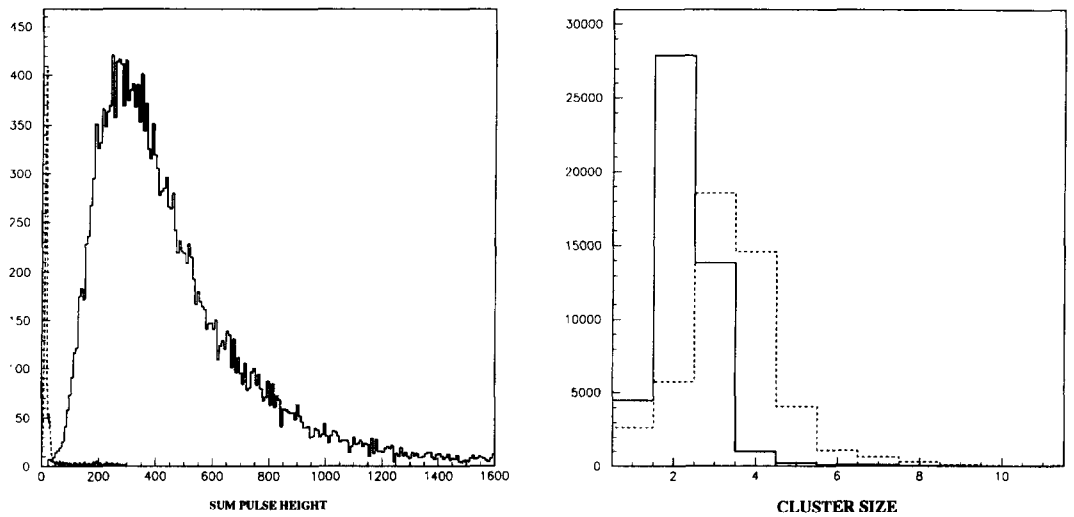

Fig. 2. (a) Total cluster and noise amplitude distributions. (b) Cluster size distribution before (solid line) and after (dotted line) *reverse charge* correction.

latch capacitor. This latch capacitor enables the chip to perform simple arithmetic operations with the analog signal such as addition or subtraction. For this test we sampled two buffers simultaneously at a frequency of 10 MHz. After trigger arrival, we performed subtraction between 2 pairs of buffers, leaving one unread capacitor in between. This corresponds to a total 400 ns time window. We chose the feedback resistor value of the preamplifier (84 ns rise-time) to have an almost ideal integrator with ~ 2.3 μs fall-time. Although with this readout scheme it is possible to wait for a trigger a long time (in our setup 3.2 μs), the use of this kind of electronics in a random trigger environment has the disadvantage of a non-synchronized sampling-to-signal. This effect produces some signal smearing because of the random displacement of the sampling clock with respect to signal arrival. Analog output from the front-end was digitized by a flash ADC SIROCCO II unit at a rate of 1 MHz.

4. Chamber performance

We selected events which fired MSGC and the fiber detector (HC) [13] (see Fig. 1) within a window of 0.5 mm, which corresponded to the scintillating fiber diameter. After pedestal subtraction, noise was rejected with a 2σ cut from the pedestal distribution. Clusters were defined with consecutive hits above threshold. The total amplitude of the clusters together with the distribution of the noise amplitude can be seen in Fig. 2. We

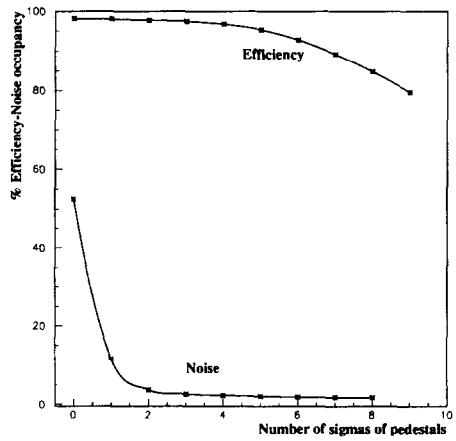

Fig. 3. Efficiency and noise occupancy.

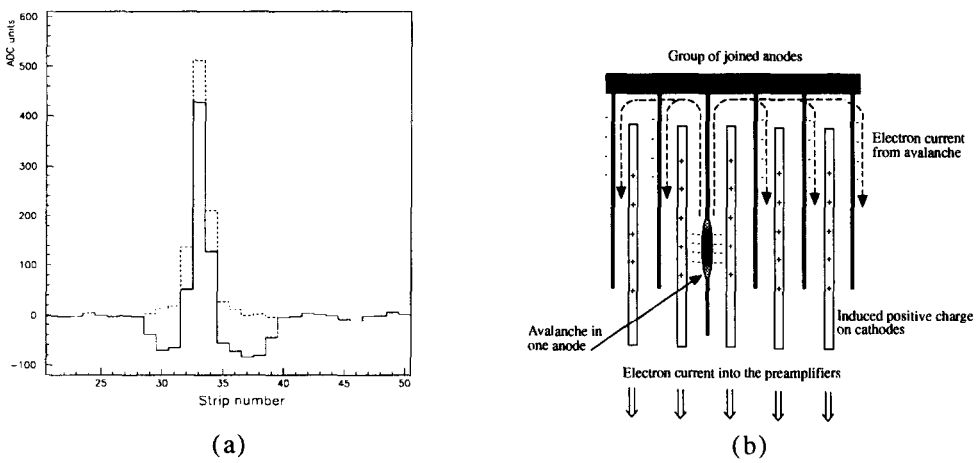

Fig. 4. (a) Hit profile of an event before (solid line) and after (dotted line) the *reverse charge* correction. (b) Illustration of the *reverse charge*.

obtained an outstanding signal-to-noise ratio of 28 (Fig. 2) for minimum ionizing particles[2]. Note that this result was achieved avoiding the use of gas mixtures with other noble gases (i.e. Ne). The efficiency was determined with the help of the HC hodoscope, and we obtained a maximum value of 98.2% (shown in Fig. 3 with the noise occupancy). 25% of the events showed accidental hits with an average hit multiplicity of 1.6 per plane. The particle flux was estimated to be 10^3 $mm^{-2}s^{-1}$.

5. Anode-to-cathode induction and cluster reconstruction

In order to control the total energy accumulated in the E-field to minimize the risks of sparks, the anode strips were joined in groups of 10 connected to the HV unit through a 1 MΩ resistor. In Fig. 4a we show a typical cluster originated by a minimum ionizing particle hit. Note there is an *undershoot* in amplitude for the channels surrounding the ones that received the avalanche. This effect [14] can be explained as follows: the avalanche in anode strips produces an excess of electrons in the group of joined anodes and also an excess

[2] Defined as the ratio of most probable amplitude of signal to the standard deviation of noise distribution.

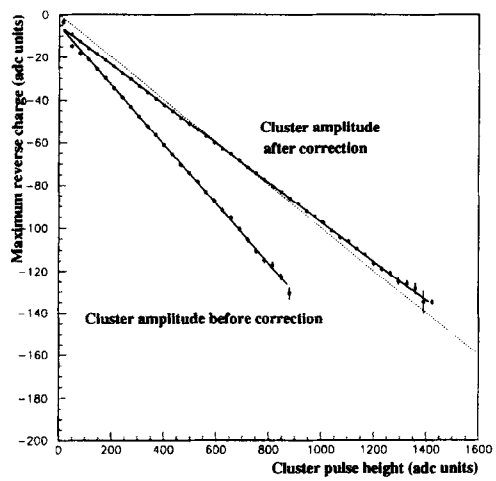

Fig. 5. Correlation between maximum *reverse charge* and the cluster amplitude. The ideal 1/10 slope (dotted straight line) expectation is also shown.

of positive charge in the adjacent cathodes. The electrons move in a *back current* towards the point in which anodes are joined, being shared by all the anodes in the group (see Fig. 4b). Subsequently this electron current induces positive charge in the adjacent cathodes, which is seen as electrons moving to the preamplifier (what we call *reverse current*). For an avalanche in a central anode of a group, the cathodes which are just between two anode groups only have one half of the maximum *reverse charge* (see Fig. 4a).

It is interesting to note that the ratio of ionic charge to the *reverse charge* is, in principle, a constant only determined by the number of coupled anode strips. Fig. 5 shows the correlation of the maximum *reverse charge* seen by the preamplifiers and the reconstructed pulse height in the cluster. In this figure we see that cluster amplitudes lie below the ideal values represented by the straight line with slope 1/10, thus indicating a defective reconstruction of the total charge in the avalanche.

In order to correct for this effect, we increase the cathode amplitudes (within one anode group) by a quantity which is given by the channel with maximal *undershoot* with respect to pedestals. After data correction the observed slope in the previous correlation is 9.2×10^{-2} (see Fig. 5) which is close to the ideal value of 1/10. A value so close to the ideal one can be explained by the signal development in the preamplifier due to its large integration time (over 90 ns), as we shall discuss later. The *reverse charge* effect could be reduced by either using a faster electronics readout or by increasing the number of HV coupled strips.

6. Optimization of pipeline readout and SPICE simulation

As we said before, analog pipeline readout has the disadvantage, within a random trigger environment, of the displacement of the sampling clock with respect to the signal development. We studied the optimization of a given sampling algorithm in order to obtain a maximum average pulse height and energy resolution. Let us assume that the signal is described by the function

$$f(\Delta, t_0, t) = \begin{cases} \dfrac{(1+\tau_2/\tau)^{\tau/\tau_2}}{(1-\tau/(\tau_2+\tau))} \exp\left(-\dfrac{x}{\tau_2}\right)\left(1-\exp\left(-\dfrac{x}{\tau}\right)\right) & \text{if } 0 < x, \\ 0 & \text{if } x \leqslant 0, \end{cases} \tag{1}$$

where τ, τ_2 are the variables that correspond to the rise and fall time and $x = t - (\Delta + t_0)$. The function $f(\Delta, t_0, t)$ is normalized to have a maximum value of 1. The sum $\Delta + t_0$ represents the actual start time of the

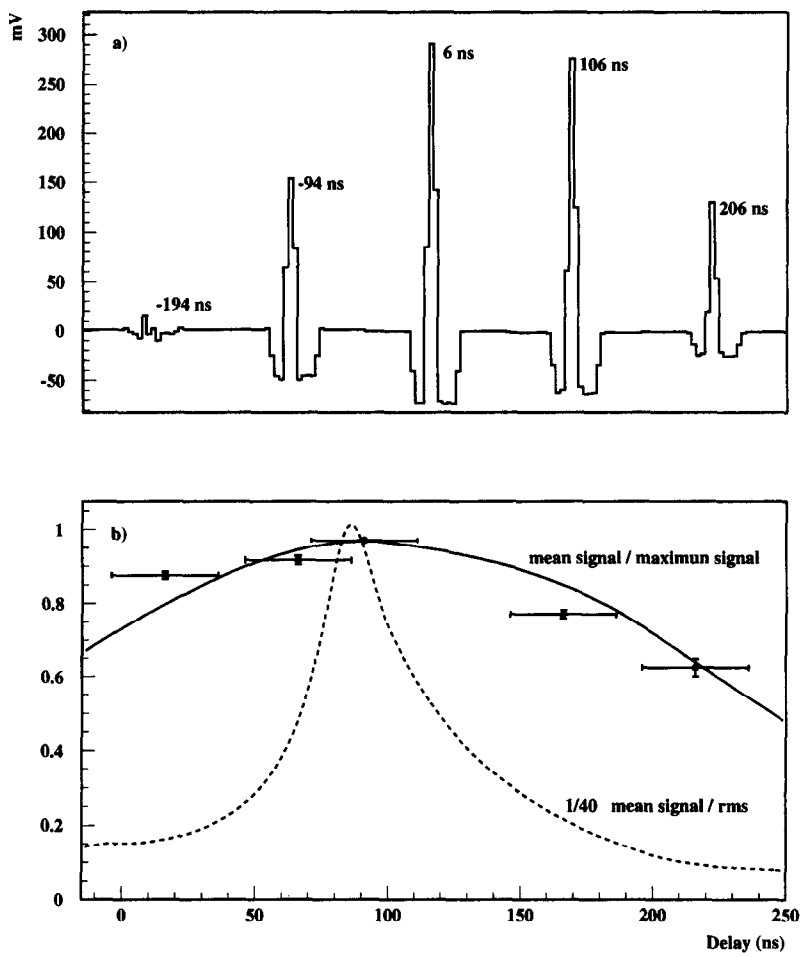

Fig. 6. (a) A SPICE simulated hit profile for five different values of t_0 for optimum value of Δ = 86 ns. (b) Mean signal normalized to its maximum value and ⟨signal⟩/rms for the analog pipeline readout versus Δ.

signal which is sampled at time t, while Δ is the overall delay of the signal (which we can control); t_0 is a random variable distributed over one sampling period α, with a probability distribution given by

$$P(t_0) = \begin{cases} 1/\alpha & \text{if } 0 < t_0 < \alpha, \\ 0 & \text{else,} \end{cases} \tag{2}$$

We can optimize the detector readout by determining the best Δ parameter for a given algorithm. For this purpose we evaluate the mean signal $\langle f \rangle$ and the mean squared signal $\langle ff \rangle$ as:

$$\langle f \rangle(\Delta, t) = \int_{-\infty}^{+\infty} P(t_0) f(\Delta, t_0, t)\, \mathrm{d}t_0 \tag{3}$$

and

Table 1
Values of parameters used for the SPICE simulation (see Fig. 7).

Rc	0.18 kΩ/cm
Ra	2.46 kΩ/cm
Rb	370 Ω
Cac	0.43 pF/cm
Ccb	0.48 pF/cm
Cab	0.12 pF/cm
Cpa	0.5 pF

$$\langle ff\rangle(\Delta,t,t') = \int_{-\infty}^{+\infty} P(t_0) f(\Delta,t_0,t) f(\Delta,t_0,t')\,\mathrm{d}t_0, \tag{4}$$

where the explicit expressions can be found in the appendix. In the algorithm used for this analysis, the signal is given by the analog subtraction of the sum of two buffers (1st and 2nd) from the sum of other two (4th and 5th) leaving one unread buffer in between. The mean value and the rms of the readout signal are

$$\langle \text{signal}\rangle = \sum_{i\in S} \sigma(i)\langle f\rangle(\Delta, i\alpha),$$

$$(\text{rms})^2 = \sum_{i,j\in S} \langle ff\rangle(\Delta, i\alpha, j\alpha)\sigma(i)\sigma(j) - \langle \text{signal}\rangle^2,$$

$$S_1 = \{1,0\}, \qquad S_2 = \{4,3\}, \qquad S = S_1 \cup S_2,$$

$$\sigma(i) = 1, \quad i \in S_2, \qquad \sigma(i) = -1, \quad i \in S_1.$$

This can be easily extended to any other sampling algorithm. Then, we choose the optimum Δ value as the one that maximizes the ratio $\langle \text{signal}\rangle/\text{rms}$. Fig. 6 shows the expected dependence on Δ of the mean signal (normalized to its maximum value) compared to the experimental data. Fig. 6 also shows the dependence on Δ of the ratio $\langle \text{signal}\rangle/\text{rms}$ expected from the previous parametrization. For the given algorithm the optimum delay Δ is 86 ns, using the values $\alpha = 100$ ns, $\tau = 77$ ns and $\tau_2 = 1.8$ μs. Although mean signal does not depend very significantly on the delay, the width of the pulse height distribution varies considerably, thus degrading the overall energy resolution of the detector (Fig. 6).

In order to study the behaviour of the signal in the detector, we also developed a SPICE[3] simulation of the MSGC, based in an equivalent circuit with discrete elements. The scheme of the SPICE circuit is showed in Fig. 7. It can be considered as composed of four parts, i.e. MSGC (anodes, cathodes and backplane), chamber biasing (HV supply), connections (bondings and pitch adapters) and preamplifiers. A MSGC segment is simulated through a basic equivalent circuit cell. Each cell contains one anode and one cathode resistors and capacitors simulating the electrical coupling between them. Anodes are biased in groups of 10. In order to simulate the whole chamber we used four cells in series. We have checked that the results do not change significantly by including a larger number of cells. The values of the simulation parameters[4] are listed in Table 1.

The preamplifier connected to the cathode consists of two MOS transistors on inverse configuration with an RC feedback (see Fig. 8) [11]. We determined the preamplifier parameters by pulsing the backplane, and fitting the measured response ($\tau = 42$ ns and $\tau_2 = 1$ μs). The ionic charge input was simulated with two current sources from one anode to the adjacent cathodes with an exponential shape $I(t) = I_0[\exp(-t/f) - \exp(-t/r)]$ with $f = 5$ ns and $r = 1$ ns. In this way, we obtained the signal development in the preamplifiers, which is shown in Fig. 9. Taking into account the sampling algorithm described earlier, we see in Fig. 6a the simulation of the hit profile for five different values of t_0 at the optimum value of Δ. One can clearly appreciate the effect of the *reverse charge* which compares very well with the real data shown in Fig. 4.

[3] SPICE 3f4 U.C. Berkeley CA.

[4] Measured with a HP 4284A LCR meter and a Karl-Suss micro-probe platform.

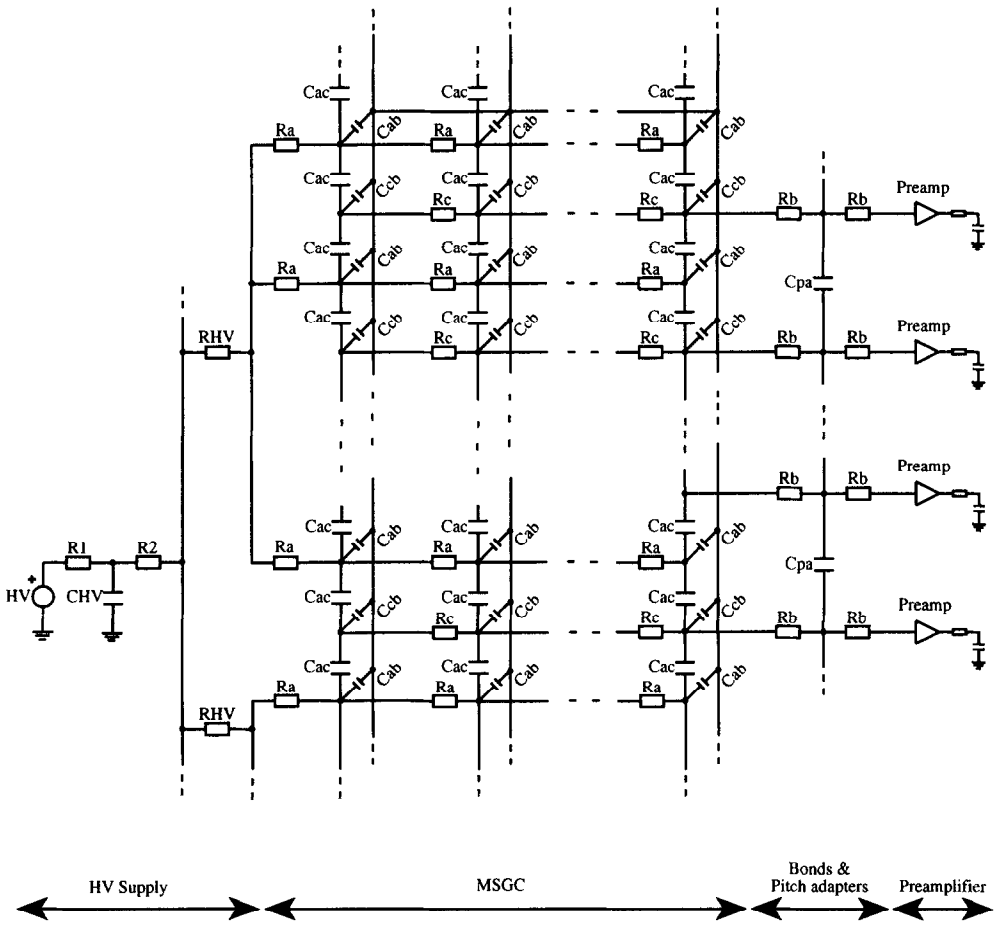

Fig. 7. SPICE equivalent circuit of the MSGC plane.

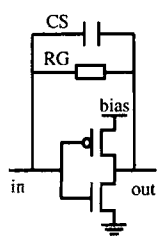

Fig. 8. Model circuit of the preamplifier.

7. Conclusions

We have studied the performance of a Microstrip Gas Chamber with analog pipeline readout in a random trigger setup. We have demonstrated the possibility of operation with excellent efficiency and signal-to-noise ratio in a 50%–50% mixture of Ar–DME. We give the algorithm for optimization of the signal distribution versus trigger delay, and simulated the electrical response of the detector including the front-end preamplifiers.

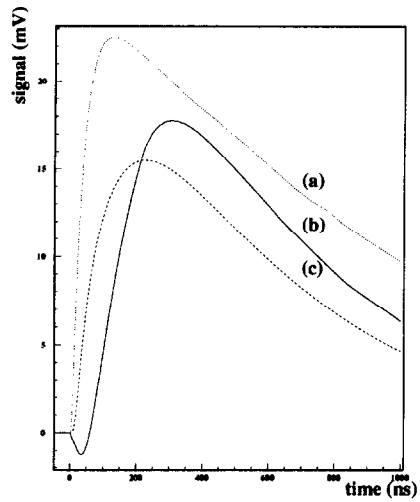

Fig. 9. Time development of the signal in MSGC: (a) pulsing the backplane. (b) cathode signal from an avalanche 8 cm away from preamplifier. (c) same as (b) for a few mm distance.

Acknowledgements

We are grateful to F. Sauli and the GDD CERN group for their invaluable help; specially to M. Capeans, L. Ropelewski and C. Garabatos. Also we want to express our gratitude to R. Horisberger and F. Hartjes for their assistance in this work. Finally, also we thank K. Kuroda, I. Manuilov, S. Trusov and the RD17 group for their collaboration in the test beam.

Appendix A

Using expressions (1) and (2), we can compute the values of $\langle f \rangle$ and $\langle ff \rangle$ as mentioned in Section 6:

$$\langle f \rangle(\Delta, t) = \int_{-\infty}^{+\infty} P(t_0) f(\Delta, t_0, t)\, \mathrm{d}t_0$$

$$= \begin{cases} \dfrac{A}{\alpha} \exp\left(-\dfrac{(t-\Delta)}{\tau_2}\right) \left[2\tau_2 \exp(\alpha/2\tau_2) \sinh(\alpha/2\tau_2) \right. \\ \left. -\dfrac{2\tau_2\tau}{(\tau_2+\tau)} \exp\left(\alpha/2\left(\dfrac{1}{\tau_2}+\dfrac{1}{\tau}\right)\right) \exp\left(-\dfrac{(t-\Delta)}{\tau}\right) \sinh\left(\alpha/2\left(\dfrac{1}{\tau_2}+\dfrac{1}{\tau}\right)\right)\right] \\ \quad \text{if } \Delta < t-\alpha, \\ \dfrac{A}{\alpha} \exp\left(-\dfrac{(t-\Delta)}{\tau_2}\right) \left[2\tau_2 \exp((t-\Delta)/2\tau_2) \sinh((t-\Delta)/2\tau_2) \right. \\ \left. -\dfrac{\tau_2\tau}{(\tau_2+\tau)} \left(\exp\left(-\dfrac{(t-\Delta)}{\tau_2}\right) - \exp\left(-\dfrac{(t-\Delta)}{\tau}\right)\right)\right] \\ \quad \text{if } t-\alpha \leqslant \Delta < t, \\ 0 \quad \text{if } t \leq \Delta \end{cases}$$

and

$$\langle ff\rangle(\Delta,t,t') = \int_{-\infty}^{+\infty} P(t_0) f(\Delta,t_0,t) f(\Delta,t_0,t')\,\mathrm{d}t_0$$

$$= \begin{cases} \dfrac{A^2}{\alpha}\exp\left(\dfrac{-(t+t'-2\Delta)}{\tau_2}\right)\left[\tau_2\exp\left(\dfrac{\alpha}{\tau_2}\right)\sinh\left(\dfrac{\alpha}{\tau_2}\right)\right. \\ -\dfrac{2\tau\tau_2}{\tau_2+2\tau}\exp\left(\dfrac{\alpha(\tau_2+2\tau)}{2\tau_2\tau}\right)\sinh\left(\dfrac{\alpha(\tau_2+2\tau)}{2\tau_2\tau}\right)\exp\left(\dfrac{\Delta}{\tau}\right)\left(\exp\left(\dfrac{-t}{\tau}\right)+\exp\left(\dfrac{-t'}{\tau}\right)\right) \\ \left.+\dfrac{\tau\tau_2}{\tau_2+\tau}\exp\left(\alpha\dfrac{\tau_2+\tau}{\tau\tau_2}\right)\sinh\left(\alpha\dfrac{\tau_2+\tau}{\tau\tau_2}\right)\exp\left(\dfrac{-(t+t'-2\Delta)}{\tau}\right)\right] \\ \quad \text{if } \Delta < t'-\alpha, \\ \dfrac{A^2}{\alpha}\exp\left(\dfrac{-(t+t'-2\Delta)}{\tau_2}\right)\left\{\tau_2\exp\left(\dfrac{t'-\Delta}{\tau_2}\right)\sinh\left(\dfrac{t'-\Delta}{\tau_2}\right)\right. \\ -\dfrac{\tau\tau_2}{\tau_2+2\tau}\left[\exp\left(\dfrac{-2\Delta}{\tau_2}\right)\exp\left(t'\dfrac{\tau_2+2\tau}{\tau_2\tau}\right)-\exp\left(\dfrac{\Delta}{\tau}\right)\right]\left[\exp\left(\dfrac{-t}{\tau}\right)+\exp\left(\dfrac{t'}{\tau}\right)\right] \\ \left.+\dfrac{\tau\tau_2}{\tau_2+\tau}\left[\exp\left((t'-\Delta)\dfrac{\tau_2+2\tau}{\tau\tau_2}\right)-\exp\left(-\dfrac{t'-\Delta}{\tau}\right)\right]\exp\left(-\dfrac{t-\Delta}{\tau}\right)\right\} \\ \quad \text{if } t'-\alpha \le \Delta \le t', \\ 0 \quad \text{if } t' \le \Delta \end{cases}$$

with

$$A = \frac{(1+\tau_2/\tau)^{\tau/\tau_2}}{(1-\tau/(\tau_2+\tau))}$$

and assuming $t' \leqslant t$.

References

[1] Lifetime measurement of $\pi^+\pi^-$ atoms to test low energy QCD predictions, CERN/SPSLC 95-1, DIRAC PROPOSAL.
[2] A. Oed, Nucl. Instr. and Meth. A 263 (1988) 351.
[3] F. Angellini, R. Bellazzini, A. Brez, M.M. Massai, G. Spandre and M.R. Torquati, Nucl. Instr. and Meth. A 283 (1989) 755.
[4] R. Bouclier, M. Capeáns, G. Million, L. Ropelewski, F. Sauli, T. Temmel, R.A. Cooke, S. Donnel, S.A. Sastri and N. Sonderer, CERN-PPE/95-95.
[5] W.G. Gong, R. Bellazzini, A. Brez, R. Raffo and G. Spandre, Nucl. Instr. and Meth. A 374 (1996) 144.
[6] F. Angellini, R. Bellazzini, A. Brez, M.M. Massai, R. Raffo, M.A. Spezziga, G. Spandre, M. Bozzo and A. Toropin, Nucl. Instr. and Meth. A 360 (1995) 22.
[7] F.D. van den Berg, C. Daum, B. van Eijk, F.G. Hartjes, F. Udo and V. Zhukov, Proc. Int. Workshop on MSGC, Lyon (1995) p. 285.
[8] R. Bouclier, M. Capeáns, C. Garabatos, G. Manzin, G. Million, L. Ropelewski, F. Sauli, L. Shekhtman, K. Silander and T. Ropelewski-Temmel, CERN-PPE/96-33.
[9] LDRB Status Report/RD-28, CERN/LHCC 96-18.
[10] J.E. Bateman and J.F. Connolly, RAL-TR-95-032.
[11] R. Horisberger and D. Pitzl, Nucl. Instr. and Meth. A 326 (1993) 92.
[12] F. Gómez, A. Pazos, M. Pló, B. Adeva and R. Horisberger, Proc. Int. Workshop on Micro-Strip Gas Chambers, Legnaro (1994).
[13] K. Kuroda et al., Nucl. Instr. and Meth. A 300 (1991) 259.
[14] R. Bouclier, M. Capeans, C. Garabatos, G. Manzin, A. Peisert, L. Ropelewski, F. Sauli, J.C. Santiard, L.I. Shekhtman, T. Temmel and G. Fischer, Proc. Int. Workshop on Micro-Strip Gas Chambers, Legnaro (1994).